

Published in final edited form as:

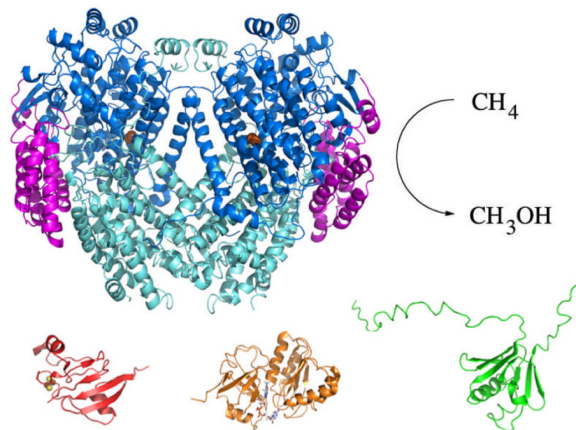
*Acc Chem Res.* 2011 April 19; 44(4): 280–288. doi:10.1021/ar1001473.

## Dioxygen Activation in Soluble Methane Monooxygenase

Christine E. Tinberg and Stephen J. Lippard\*

Department of Chemistry, Massachusetts Institute of Technology, Cambridge, MA 02139

### CONSPECTUS



The controlled oxidation of methane to methanol is a chemical transformation of great industrial importance that is underutilized because of inefficient and costly synthetic procedures. Methane monooxygenase enzymes (MMOs) from methanotrophic bacteria achieve this chemistry efficiently under ambient conditions. In this Account we discuss the first step in the oxidation of methane at the carboxylate-bridged diiron active site of the soluble MMO (sMMO), namely, the reductive activation of atmospheric  $O_2$ . The results provide benchmarks against which the dioxygen activation mechanisms of other bacterial multicomponent monooxygenases can be measured.

Molecular oxygen reacts rapidly with the reduced, diiron(II) center of the hydroxylase component of sMMO (MMOH). The first spectroscopically characterized intermediate that results from this process is an antiferromagnetically coupled peroxodiiron(III) species,  $P^*$ , in which the iron atoms have identical environments.  $P^*$  converts to a second peroxodiiron(III) unit,  $H_{\text{peroxo}}$ , in a process accompanied by the transfer of a proton, probably with the assistance of a residue near the active site. Proton-promoted O–O bond scission and rearrangement of the diiron core then leads to a diiron(IV) unit termed Q that is directly responsible for the oxidation of methane to methanol. In the first half of this Account we provide a detailed discussion of these processes, with particular emphasis on possible structures of the intermediates. The geometries of  $P^*$  and  $H_{\text{peroxo}}$  are currently unknown, and recent synthetic modeling chemistry has highlighted the need for further structural characterization of Q, previously assigned as a di( $\mu$ -oxo)diiron(IV) ‘diamond core’.

In the second half of the Account, we discuss in detail proton transfer during the  $O_2$  activation events. The role of protons in promoting O–O bond cleavage, thereby initiating the conversion of  $H_{\text{peroxo}}$  to Q, was previously a controversial topic. Recent studies performed over a range of pH values and in  $D_2O$  instead of  $H_2O$  confirmed conclusively that the transfer of protons, possibly at

\*To whom correspondence should be addressed. lippard@mit.edu. Telephone: (617) 253-1892. Fax: (617) 258-8150..

or near the active site, is necessary for both P\* to H<sub>peroxo</sub> and H<sub>peroxo</sub> to Q conversions. Specific mechanistic insights into these processes are provided.

In the last section of the Account we present our view of experiments that need to be done to further define crucial aspects of sMMO chemistry. Here our goal is to provide the reader with the challenges that we and others face in this research, particularly with respect to some longstanding questions about the system, as well as approaches that might be used to solve them.

## INTRODUCTION

A current challenge in renewable energy is the development of processes that allow us to generate alternative fuels in a sustainable manner. Methane gas is an abundant precursor of liquid fuels, but current strategies for its selective conversion to methanol, a necessary step in its utilization, are neither economical nor sustainable.<sup>1</sup> Methanotrophic bacteria utilize methane as a sole carbon source. The first step in the metabolism of methane by these organisms is its selective conversion to methanol by methane monooxygenase enzymes (MMOs) (eq 1). Two methane monooxygenases have evolved to



perform this reaction: a membrane-bound particulate MMO (pMMO) present in most methanotrophs, and a soluble MMO (sMMO) expressed in several methanotrophs under copper-limited conditions. Both MMOs utilize a metal center to activate atmospheric dioxygen for attack on the strong C–H bond (104 kcal/mol) of methane. Although the active site of pMMO is probably a dinuclear copper center,<sup>2</sup> that of sMMO is a carboxylate-bridged diiron unit.<sup>3,4</sup> The oxidative chemistry performed at these sites, particularly the latter, has been investigated extensively, elevating our understanding of how Nature utilizes biological methane as an energy source and guiding the development of industrially relevant small molecule catalysts.<sup>5</sup> In this Account we review recent progress toward understanding biological methane oxidation at the diiron center of sMMO. A groundbreaking study of pMMO is available in the recent literature.<sup>2</sup>

### Soluble Methane Monooxygenase

sMMO has been studied primarily in two methanotrophs, *Methylococcus capsulatus* (Bath), hereafter referred to as *Mc*, and *Methylosinus trichosporium* OB3b, hereafter *Mt*. Methane oxidation occurs at a carboxylate-bridged diiron center housed within a hydroxylase protein (MMOH) featuring an ( $\alpha\beta\gamma$ )<sub>2</sub> dimer architecture.<sup>6</sup> The catalytic active site resides in a four-helix bundle of the  $\alpha$ -subunit. The diiron center is coordinated by two histidine and four glutamate ligands (Figure 1). Solvent-derived molecules complete the pseudo-octahedral coordination spheres. In the diiron(III) resting state of the enzyme (MMOH<sub>ox</sub>), two hydroxide ligands bridge the iron atoms, which are separated by ~3.1 Å (Figure 1a).<sup>6</sup> Upon reduction to the diiron(II) form (MMOH<sub>red</sub>), the bridging solvent molecules depart and E243, which is bound only to Fe1 in MMOH<sub>ox</sub>, assumes a bridging position while remaining chelated to Fe2 (Figure 1b). As a consequence, an open coordination site becomes available and the Fe–Fe distance increases.<sup>7</sup>

The structural features of MMOH<sub>ox</sub> and MMOH<sub>red</sub> have been investigated by EXAFS, EPR, ENDOR/ESEEM, MCD, and Mössbauer spectroscopy.<sup>3,4</sup> The high-spin Fe(III) ions of MMOH<sub>ox</sub> are antiferromagnetically coupled, resulting in a diamagnetic ground state. Two hydroxide bridges mediate the spin-exchange. In contrast, the high-spin Fe(II) atoms of MMOH<sub>red</sub> are weakly ferromagnetically coupled and the resulting  $S = 4$  spin system has a

low energy Kramer's doublet that is split in zero applied field, giving rise to a characteristic EPR signal at  $g = 16$ .

### The Reaction of $\text{MMOH}_{\text{red}}$ with $\text{O}_2$

The reductive activation of  $\text{O}_2$  at the diiron(II) center of  $\text{MMOH}_{\text{red}}$  is the first step of the sMMO catalytic cycle (Figure 2). Despite the observation that the diiron active site is buried within the MMOH hydrophobic protein environment,  $\text{O}_2$  can access it in a facile manner. The route of  $\text{O}_2$  delivery to the active site has been suggested by structural studies. Crystallographic investigations of MMOH revealed several adjacent hydrophobic cavities in the  $\alpha$ -subunit that delineate a pathway from the exterior of the protein to the diiron site (Figure 3).<sup>6</sup> Crystals of MMOH pressurized with xenon gas, an electron-rich  $\text{O}_2$  and  $\text{CH}_4$  surrogate, contained ordered Xe atoms residing almost exclusively in these cavities, suggesting a route by which these substrates might access the active site.<sup>8</sup> An alternative method of substrate ingress and/or product egress is through a pore formed between two of the helices that ligate the diiron center (Figure 3). Hydrophilic residues line the pore, which has been proposed as a pathway of  $\text{H}_3\text{O}^+$  translocation.<sup>9</sup>

Upon reaching the diiron(II) center,  $\text{O}_2$  rapidly reacts in the presence of two equivalents of the regulatory protein MMOB.<sup>10,11</sup> The rate constant for  $\text{O}_2$ -promoted  $\text{MMOH}_{\text{red}}$  decay was measured to be  $\sim 24 \text{ s}^{-1}$  at pH 7.0 and  $4^\circ\text{C}$  by rapid freeze-quench (RFQ) Mössbauer spectroscopy in *Mc* MMOH<sup>11</sup> and  $\sim 22 \text{ s}^{-1}$  at pH 7.7 and  $4^\circ\text{C}$  by RFQ EPR spectroscopy in *Mt* sMMO.<sup>10</sup> For *Mt*  $\text{MMOH}_{\text{red}}$ , this process is independent of pH and  $[\text{O}_2]$  between 0.3 and 0.7 mM. One interpretation of these results is that a rapid, irreversible  $\text{O}_2$  binding event precedes oxidation of the diiron center.<sup>10</sup> Alternatively,  $\text{O}_2$  binding might involve a reversible pre-equilibrium followed by an irreversible chemical reaction with the Michealis constant ( $K_M$ ) being much lower than the concentrations of  $\text{O}_2$  used in the EPR experiments such that the system is saturated.<sup>12</sup> An attempt to find such evidence in *Mc* MMOH using an oxygen electrode failed to detect a tight enzyme-dioxygen interaction, however.<sup>12</sup> It is possible that an irreversible conformational change precedes reaction of  $\text{O}_2$  at the diiron center.<sup>13</sup>

### Peroxodiiron(III) Intermediates of MMOH

Computational studies suggest that the first intermediate resulting from reaction of  $\text{MMOH}_{\text{red}}$  with  $\text{O}_2$  is a mixed-valent diiron(II/III) superoxide species.<sup>14,15</sup> An oxygen KIE study of sMMO oxidation of  $\text{CH}_3\text{CN}$  returned a value of 1.016, consistent with one-electron reduction of  $\text{O}_2$  to superoxide being the first irreversible step in the reaction pathway, although other possibilities could not be definitively ruled out.<sup>12</sup> An Fe(II)/Fe(III) superoxide unit has never been directly observed in a diiron enzyme in which the  $\text{O}_2$ -activating species is diiron(II), however, most likely because of its transient existence.<sup>16,17</sup>

The first spectroscopically observed intermediate in the reaction of  $\text{MMOH}_{\text{red}}$  with  $\text{O}_2$  is a peroxodiiron(III) species. Early kinetic evidence for this unit was provided by studies of the *Mt* system, because the rate constant for  $\text{O}_2$ -promoted  $\text{MMOH}_{\text{red}}$  decay was significantly faster than that describing formation of the earliest observed oxygenated-iron species arising from the reaction, intermediate Q (vide infra).<sup>10</sup> These observations indicated the presence of at least one additional intermediate preceding Q formation. The first direct spectroscopic evidence for such a transient came from studies of *Mc* MMOH.<sup>11,18</sup> The 4.2 K Mössbauer spectrum of this intermediate, termed  $\text{H}_{\text{peroxo}}$ ,<sup>19</sup> revealed a diamagnetic center having similar iron(III) sites.<sup>18,20</sup> Stopped-flow UV-vis analyses revealed a rich optical profile having distinct features at 420 nm and 720 nm (Table 1).<sup>21</sup> RFQ Mössbauer and stopped-flow optical spectroscopic studies yielded the same decay rate constant for this intermediate ( $\sim 0.36 \text{ s}^{-1}$  at  $4^\circ\text{C}$ ); however, the kinetic parameter describing its formation was found to be

different by the two techniques. RFQ Mössbauer experiments returned a rate constant of  $\sim 25 \text{ s}^{-1}$  at  $4 \text{ }^\circ\text{C}$ , a value in agreement with that measured for  $\text{MMOH}_{\text{red}}$  decay (vide supra).<sup>11</sup> In contrast, stopped-flow studies indicated a value of  $\sim 1 \text{ s}^{-1}$  at  $4 \text{ }^\circ\text{C}$ .<sup>21,22</sup> Two distinct peroxodiiron(III) species having similar Mössbauer parameters but distinct optical signatures were proposed to explain the discrepancy.<sup>21</sup>

The first evidence for two peroxodiiron(III) intermediates was provided by stopped-flow optical studies of the *Mt* enzyme.<sup>23</sup> Fits of data monitoring the reaction of  $\text{MMOH}_{\text{red}}$  with  $\text{O}_2$  in the presence of MMOB at 430 nm required an additional phase preceding  $\text{H}_{\text{peroxo}}$  formation. The species assigned to this phase, P\*, formed with a rate constant of  $\sim 22 \text{ s}^{-1}$  at  $4 \text{ }^\circ\text{C}$ , consistent with it being the first intermediate resulting from decay of  $\text{MMOH}_{\text{red}}$ . From the amplitudes of the kinetic phases revealed by these studies,  $\text{H}_{\text{peroxo}}$ , with  $k_{\text{form}} = 9\text{--}12 \text{ s}^{-1}$  at  $4 \text{ }^\circ\text{C}$  and pH 7.0, was suggested to have negligible absorbance at 430 nm, an observation inconsistent with that for *Mc* MMOH (vide supra). The authors explained this contradiction by proposing that the signal detected at 420 nm for *Mc*  $\text{H}_{\text{peroxo}}$  was an artifact of the dominant optical contribution of Q at this wavelength.<sup>23</sup> We recently obtained direct optical spectroscopic evidence for P\* in *Mc* MMOH,<sup>24</sup> which shows distinct features at 720 nm ( $\epsilon \approx 1250 \text{ M}^{-1} \text{ cm}^{-1}$ ) and 420 nm ( $\epsilon \approx 3500 \text{ M}^{-1} \text{ cm}^{-1}$ ). The latter was clearly revealed when reactions were performed in the presence of high concentrations of  $\text{CH}_4$  to eliminate the optical contribution of Q at this wavelength. These studies provide conclusive evidence that  $\text{H}_{\text{peroxo}}$  does indeed absorb at 420 nm. This conclusion is important for comparing the properties of  $\text{H}_{\text{peroxo}}$  to those of synthetic peroxodiiron(III) complexes and computational models for the intermediate.

From the similarities in Mössbauer parameters (vide supra) and optical properties to those of  $\text{H}_{\text{peroxo}}$ , we proposed that P\* features an identical  $\text{Fe}_2\text{O}_2$  core but differs instead in the conformation of the supporting ligands. The exact structures of the sMMOH peroxodiiron(III) species remain a major unsolved question in the field, however. Several possible architectures differing in the geometry of the  $\{\text{Fe}_2\text{O}_2\}^{4+}$  unit as well as the coordination state of E243 are depicted in Figure 4.

Structural insights can be gleaned from comparing the spectroscopic parameters of P\* and  $\text{H}_{\text{peroxo}}$  to those of peroxodiiron(III) intermediates of similar diiron enzymes (Table 1). Peroxide units forming in several of these proteins, including the R2 subunit of ribonucleotide reductase (RNR-R2), have been structurally characterized by resonance Raman (RR) spectroscopy, which indicates a  $\mu$ -1,2 peroxide binding mode (**1** – **4**) in all cases.<sup>25–29</sup> A *cis*- $\mu$ 1,2-peroxide coordination geometry (**1** or **2**) was also suggested from the X-ray crystal structure of the toluene 4-monooxygenase hydroxylase-regulatory protein complex soaked with  $\text{H}_2\text{O}_2$ .<sup>30,31</sup> X-ray crystal structures of several peroxodiiron(III) model compounds are available (Table 1).<sup>5,32</sup> One in particular has Mössbauer parameters that are nearly identical to those of P\*,  $[\text{Fe}_2(\mu\text{-}1,2\text{-O}_2)(\mu\text{-O}_2\text{CCH}_2\text{Ph})_2\{\text{HB}(\text{pz}')_3\}_2]$ , where *pz'* is 3,5-bis(isopropyl)-pyrazolyl. The crystal structure of this complex reveals a *gauche*  $\mu$ -1,2 peroxide configuration (**3** or **4**) (Table 1).<sup>33</sup> High-level theoretical calculations also favor a *gauche*  $\mu$ -1,2-peroxo structure for  $\text{H}_{\text{peroxo}}$ .<sup>34</sup> Although a nonplanar  $\mu$ - $\eta^2$ : $\eta^2$  geometry (**7**) has also been suggested,<sup>14,15,35</sup> it is no longer favored computationally.<sup>36</sup>

## Intermediate Q

$\text{H}_{\text{peroxo}}$  can oxidize electron-rich substrates.<sup>21,37,38</sup> In the absence of such substrates, cleavage of the O–O bond results in its rapid conversion to intermediate Q, an antiferromagnetically coupled diiron(IV) unit with absorption bands at  $\sim 350$  and  $\sim 420$  nm (Table 2).<sup>10,11,18,39</sup> The rate constants for this process are  $0.36 \text{ s}^{-1}$  and  $2.5 \text{ s}^{-1}$ , respectively, for the *Mc*<sup>24</sup> and *Mt*<sup>23</sup> enzymes at  $4 \text{ }^\circ\text{C}$  and pH 7.0. The single quadrupole doublet observed in the Mössbauer spectrum of *Mt* Q suggested similar ligand environments for both Fe(IV)

atoms (Table 2).<sup>39</sup> In contrast, two equal-intensity quadrupole doublets were detected for *Mc* Q.<sup>11,18</sup> An EXAFS spectrum of *Mt* Q was interpreted in terms of a di( $\mu$ -oxo)diiron(IV) 'diamond core' structure with a short Fe–Fe distance of 2.46 Å and Fe–O bond lengths of 1.77 Å and 2.05 Å at each iron atom (Figure 5, 9).<sup>20</sup> Recent quantum mechanics/molecular mechanics (QM/MM) studies suggest that the short Fe–Fe distance of Q might reflect protein-based compression along the Fe–Fe vector, which provides the necessary driving force to generate the intermediate.<sup>15</sup> Based on the EXAFS parameters the authors proposed a head-to-tail dimer of Fe<sup>IV</sup>=O units having an additional carboxylate bridge to reconcile the unusually short Fe–Fe bond distance compared to synthetic model complexes with {Fe<sub>2</sub>O<sub>2</sub>}<sup>n+</sup> core structures (Table 2). The inability of the sole di( $\mu$ -oxo)diiron(IV) model complex<sup>40</sup> and various high-level density functional theory (DFT) calculations<sup>14,15</sup> to reproduce the short Fe–Fe bond distance underscores the need for further structural characterization of this intermediate.

The reactivity patterns of several model complexes also suggest reconsideration of the proposed structure of Q. Reaction of [Fe<sub>2</sub>(H<sub>2</sub>Hbamb)<sub>2</sub>(*N*-meIm)<sub>2</sub>], where H<sub>4</sub>Hbamb is 2,3-*bis*(2-hydroxybenzamido)-dimethylbutane and meIm is *N*-methylimidazole, with oxygen atom donors resulted in formation of a diiron(II/IV) complex having a terminal Fe<sup>IV</sup>=O unit capable of oxidizing cyclohexane to cyclohexanol.<sup>41</sup> In this example, the potency of the system was achieved by concentrating the oxidizing capability at the Fe(IV) center. The authors proposed that an analogous diiron(III/V) center (**10**) might be responsible for methane oxidation in MMOH. A separate investigation found that the valence-localized [OH–Fe<sup>III</sup>–O–Fe<sup>IV</sup>=O]<sup>2+</sup> form of a synthetic complex supported by *tris*((4-methoxy-3,5-dimethyl-pyridin-2-yl)methyl)amine cleaves strong C–H bonds a million-fold faster than its valence-delocalized [Fe<sup>3.5</sup>( $\mu$ -O)<sub>2</sub>Fe<sup>3.5</sup>]<sup>3+</sup> 'diamond core' analogue.<sup>42</sup> A third study revealed the rate of 9,10-dihydroanthracene oxidation by [Fe<sup>IV</sup><sub>2</sub>( $\mu$ -O)<sub>2</sub>L<sub>2</sub>]<sup>4+</sup>, where L = *tris*((4-methoxy-3,5-dimethylpyrid-2-yl)*d*<sub>2</sub>-methyl)amine, to be significantly slower for than that by [Fe<sup>IV</sup>(O)(L)(NCMe)]<sup>2+</sup>, the corresponding mononuclear Fe<sup>IV</sup>=O complex of the same ligand.<sup>40</sup> Together, these data suggest that an oxidant with a terminal Fe=O unit (**11** or **12**) might be more effective for C–H bond cleavage than one having an oxo-bridged Fe–O–Fe center and indicate that further structural characterization of Q is necessary to understand better how this intermediate hydroxylates methane. RFQ coupled with advanced spectroscopic methods such as cryoreduction/ENDOR, resonance Raman, and possibly nuclear resonance vibrational spectroscopy, can aid in characterizing Q. To date, application of these methods to the intermediates of MMO has proved difficult, however. Advances in spectroscopic methodology and possibly sample preparation may help to overcome past failures.

One point regarding the structure of Q that requires further consideration is whether the RFQ-trapped intermediate studied by EXAFS spectroscopy is the same species identified in stopped-flow kinetic studies.<sup>41</sup> To activate the strong C–H bond of methane, Q must be an extremely potent oxidant; however, its oxidizing power must be controlled to prevent oxidative damage to the protein. Given recent biomimetic findings (*vide supra*), it is not unlikely that Q collapses to a more thermodynamically stable species, such as a 'diamond core', to protect the enzyme from self-destruction in the absence of substrate. It is therefore necessary to prove that RFQ-trapped samples of Q are chemically competent.

Q reacts rapidly with methane and other substrates.<sup>10,21,23,43</sup> Mechanistic considerations are reviewed elsewhere.<sup>44</sup> In the absence of substrate, Q decays by acquiring two electrons and two protons to regenerate MMOH<sub>ox</sub>. The mechanism of this transformation is largely unknown, but recent kinetic studies of *Mc* MMOH have identified a species, Q\*, that lies on this pathway.<sup>24</sup> Q\* displays a unique shoulder at 455 nm in its optical spectrum and has a



decay rate constant unaffected by CH<sub>4</sub>. Additional spectroscopic properties of this species have not been determined.

### The Role of Protons During O<sub>2</sub> Activation

The role of protons during sMMO O<sub>2</sub> activation has been a controversial topic. Early studies on cytochrome P450s, heme monooxygenases that activate strong C–H bonds in a fashion similar to sMMO, revealed that sequential transfer of two protons to the distal oxygen atom of a dioxygen unit bound terminally to the iron center provides the driving force for heterolytic O–O bond cleavage. This event results in the release of a water molecule and formation of the iron(IV)-ligand radical species responsible for the hydroxylation chemistry.<sup>45</sup> Based on these findings, a similar type of mechanism was envisioned for sMMO (Figure 6a).

The first studies probing proton involvement in sMMO, performed by our group, demonstrated that proton transfer is not rate-determining for any of the O<sub>2</sub> activation events, including O–O bond cleavage.<sup>11</sup> We employed stopped-flow optical spectroscopy to probe the proton-dependences of the events that occur upon rapidly mixing a solution of *Mc* MMOH<sub>red</sub> and MMOB prepared in 10 mM MOPS at pH 7.0 with O<sub>2</sub>-saturated 100 mM buffer having the desired reaction pH.<sup>11</sup> Using this method, all of the O<sub>2</sub> activation processes monitored were independent of pH between pH 6.6 and 8.6 at 4 °C. An examination of the same reaction in D<sub>2</sub>O showed a negligible effect of isotopic substitution.<sup>11,46</sup> Together these two observations suggested that proton transfer is not rate determining for any of the processes monitored. We proposed a mechanism involving proton-independent, homolytic O–O bond cleavage (Figure 6b), although the studies did not rule out the possibility that fast proton transfer (i.e. not rate-determining) did occur during the steps investigated.

Subsequent, contrasting findings were reported for *Mt* MMOH.<sup>47</sup> The authors of these studies also utilized stopped-flow optical spectroscopy to investigate the effects of pH and D<sub>2</sub>O on events resulting from the reaction of MMOH<sub>red</sub> and MMOB with O<sub>2</sub>-saturated buffer in the presence of MMOB. For pH dependence experiments, protein samples were preincubated at the desired reaction pH. The experiments revealed that H<sub>peroxo</sub> formation and H<sub>peroxo</sub> to Q conversion, but not Q decay, were pH-dependent between pH 6.5 and 8.6 at 4 °C. Both pH-dependent processes displayed sigmoidal pH rate profiles revealing negligible activity at high pH. That for H<sub>peroxo</sub> formation was fit to the mathematical description of Scheme 1, model i, describing a single, reversible ionization of P\* followed by irreversible conversion to H<sub>peroxo</sub>. A pK<sub>a</sub> value of 7.6 was assigned from the data fit. Similarly, the pH rate profile of Hperoxo to Q conversion was fit to the equation describing Scheme 1, model ii, with a pK<sub>a</sub> of 7.6.

A second piece of evidence that protons played an important role during O<sub>2</sub> activation was the observation that experiments performed in D<sub>2</sub>O returned kinetic solvent isotope effects (KSIEs) of  $k_H/k_D = 1.3 \pm 0.1$  for H<sub>peroxo</sub> formation and  $1.4 \pm 0.1$  for H<sub>peroxo</sub> to Q conversion. Proton inventory plots constructed by measuring the rate constants in varying mole fractions of D<sub>2</sub>O were linear for both processes, suggesting that a single proton is transferred in the transition state for each step. This observation was interpreted as evidence that the proton transfer reactions occur at the active site and do not result from protein-based conformational or complexation changes, because the latter are likely to involve multiple proton transfers. Building from analogy to the cytochrome P450 monooxygenases and observing that the measured pK<sub>a</sub> values and proton inventory fractionation factors were consistent with a coordinated water molecule, the authors suggested the mechanism of Figure 6a.

We recently reexamined O<sub>2</sub> activation in the *Mc* system.<sup>24</sup> Experiments were performed by rapidly mixing a solution of MMOH<sub>red</sub> and MMOB pre-equilibrated at the appropriate pH with O<sub>2</sub>-saturated buffer. The data showed conclusively that proton transfer is rate determining for P\* to H<sub>peroxo</sub> and H<sub>peroxo</sub> to Q conversion but not for P\* formation, Q to Q\* conversion, or Q\* decay at 4 °C. As in the *Mt* system, the pH rate profile of P\* to H<sub>peroxo</sub> conversion fit well to the analytical equation describing Scheme 1, model i, with a pK<sub>a</sub> value of 7.2. Unlike the *Mt* system, however, the pH rate profile of H<sub>peroxo</sub> to Q conversion did not fit well to the mathematical solution of Scheme 1, model ii. Instead, model iii, describing a doubly ionizing system, was necessary to fit the data. pK<sub>a</sub> values extracted from the fits were pK<sub>1</sub> = 7.9 and pK<sub>2</sub> = 7.0. A likely explanation for the differences observed in the two *Mc* experiments is the procedure employed. The early experiments relied on a pH jump instead of a preincubation. The former depends on the ability of the active site to equilibrate with the bulk solvent on the experimental timescale. Probably such was not the case, because the hydrophobic nature of the MMOH active site cavity will make it difficult for the external pH to be realized at the site of the reaction chemistry for the faster timescale of the pH jump experiment.

We also reexamined the KSIEs for the *Mc* O<sub>2</sub> activation events.<sup>24</sup> Experiments performed in D<sub>2</sub>O returned values of 2.0 ± 0.2 for P\* to H<sub>peroxo</sub> conversion and 1.8 ± 0.3 for H<sub>peroxo</sub> to Q conversion, further supporting a role for proton transfer during these steps. Based on these data, we proposed a mechanism in which proton transfer promotes O–O bond cleavage (Figure 6c). Because it is likely that E243 must dissociate from its bridging position to allow for Q formation, the recent finding that treatment of [Fe<sub>2</sub>(μ-O<sub>2</sub>)(*N*-EtHPTB)(μ-PhCO<sub>2</sub>)]<sup>2+</sup> and [Fe<sub>2</sub>(μ-O<sub>2</sub>)(*N*-EtHPTB)(μ-C<sub>6</sub>F<sub>5</sub>CO<sub>2</sub>)]<sup>2+</sup>, where HPTB is *N,N,N',N'*-tetrakis(2-benzimidazolylmethyl)-2-hydroxy-1,3-diaminopropane, with acid leads to protonation and dissociation of the bridging carboxylate instead of the peroxide moiety,<sup>48</sup> and a theoretical study showing that protonation of the RNR-R2 peroxodiiron(III) unit does not result in a stable hydroperoxide,<sup>49</sup> we proposed that the first proton is transferred to E243 instead of the peroxide unit. Additional support for this mechanism comes from the similarity between the spectroscopic properties of P\* and H<sub>peroxo</sub>, suggesting that their iron-oxygen cores are the same. The spectroscopic properties of peroxodiiron(III) and hydroperoxodiiron(III) units are expected to be different, however.<sup>49</sup>

### The Future of sMMO

Although sMMO has been a topic of intense biochemical investigation for over thirty years, many aspects of its important chemistry remain enigmatic. As with any longstanding scientific problem, the questions that remain about the system are difficult ones to answer. What are the structures of P\*, H<sub>peroxo</sub>, and Q? What makes Q such a potent oxidant and can we use that information to design new catalysts? Is it possible to engineer the system at a protein or whole-cell scale suitable for industrial production of alternative fuels and for bioremediation purposes? Given the current environmental challenges that face our society, we believe that it is crucial to continue to investigate how this catalyst works. With new findings and advances in spectroscopic tools, the coming years should bring to light a new era in sMMO chemistry.

The structure of intermediate Q and to a lesser extent those of H<sub>peroxo</sub> and P\* remain top priorities in the field. Another challenge that has hampered our understanding of this enzyme is the inability to generate sufficient quantities of soluble enzyme bearing site-directed amino acid mutations in a robust manner. Breakthroughs in the bioengineering of the system for additional biochemical and spectroscopic studies will require more fundamental knowledge of the protein factors involved in its copper-dependent transcriptional and translational regulation. An additional question central to the study of diiron proteins is what properties of MMOH cause H<sub>peroxo</sub> to spontaneously convert to Q

whereas the peroxodiiron(III) units of most other diiron enzymes do not appear to access such high valent intermediates. By addressing these questions as a community we hope to gain new insights into this important system.

## Acknowledgments

Work from our laboratory discussed in this Account was funded by grant GM032134 from the National Institute of General Medical Sciences.

## BIOGRAPHICAL INFORMATION

**Professor Stephen J. Lippard** is the Arthur Amos Noyes Professor of Chemistry at the Massachusetts Institute of Technology. His research areas lie at the interface of inorganic chemistry and biology.

**Dr. Christine E. Tinberg** received her Bachelor of Arts in chemistry from Northwestern University in 2005, where she performed research in the laboratory of Amy Rosenzweig. In 2010, Christine received her doctorate in biochemistry at the Massachusetts Institute of Technology under Prof. Lippard, investigating the reactivity of bacterial multicomponent monooxygenases.

## REFERENCES

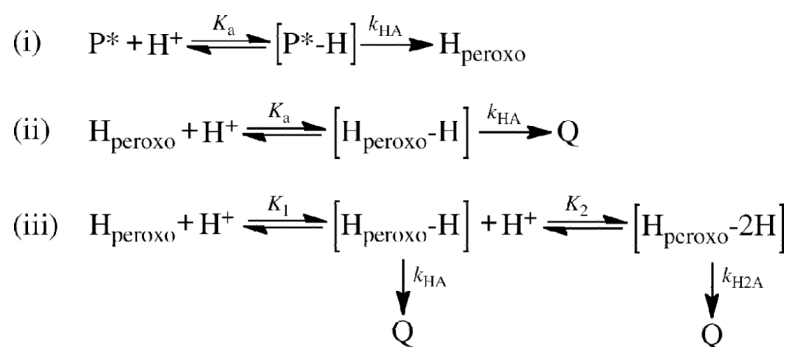
- (1). Arakawa H, Aresta M, Armor JN, Barteau MA, Beckman EJ, Bell AT, Bercaw JE, Creutz C, Dinjus E, Dixon DA, Domen K, DuBois DL, Eckert J, Fujita E, Gibson DH, Goddard WA, Goodman DW, Keller J, Kubas GJ, Kung HH, Lyons JE, Manzer LE, Marks TJ, Morokuma K, Nicholas KM, Periana R, Que L, Rostrup-Nielsen J, Sachtler WMH, Schmidt LD, Sen A, Somorjai GA, Stair PC, Stults BR, Tumas W. Catalysis Research of Relevance to Carbon Management: Progress, Challenges, and Opportunities. *Chem. Rev.* 2001; 101:953–996. [PubMed: 11709862]
- (2). Balasubramanian R, Smith SM, Rawat S, Yatsunyk LA, Stemmler TL, Rosenzweig AC. Oxidation of Methane by a Biological Dicopper Centre. *Nature.* 2010; 465:115–119. [PubMed: 20410881]
- (3). Merckx M, Kopp DA, Sazinsky MH, Blazyk JL, Müller J, Lippard SJ. Dioxygen Activation and Methane Hydroxylation by Soluble Methane Monooxygenase: A Tale of Two Irons and Three Proteins. *Angew. Chem. Int. Ed.* 2001; 40:2782–2807.
- (4). Wallar BJ, Lipscomb JD. Dioxygen Activation by Enzymes Containing Binuclear Non-Heme Iron Clusters. *Chem. Rev.* 1996; 96:2625–2657. [PubMed: 11848839]
- (5). Friedle S, Reisner E, Lippard SJ. Current Challenges of Modeling Diiron Enzyme Active Sites for Dioxygen Activation by Biomimetic Synthetic Complexes. *Chem. Soc. Rev.* 2010; 39:2768–2779. [PubMed: 20485834]
- (6). Rosenzweig AC, Frederick CA, Lippard SJ, Nordlund P. Crystal Structure of a Bacterial Non-Haem Iron Hydroxylase that Catalyses the Biological Oxidation of Methane. *Nature.* 1993; 366:537–543. [PubMed: 8255292]
- (7). Whittington DA, Lippard SJ. Crystal Structures of the Soluble Methane Monooxygenase Hydroxylase from *Methylococcus capsulatus* (Bath) Demonstrating Geometrical Variability at the Dinuclear Iron Active Site. *J. Am. Chem. Soc.* 2001; 123:827–838. [PubMed: 11456616]
- (8). Whittington DA, Rosenzweig AC, Frederick CA, Lippard SJ. Xenon and Halogenated Alkanes Track Putative Substrate Binding Cavities in the Soluble Methane Monooxygenase Hydroxylase. *Biochemistry.* 2001; 40:3476–3482. [PubMed: 11297413]
- (9). Murray LJ, Lippard SJ. Substrate Trafficking and Dioxygen Activation in Bacterial Multicomponent Monooxygenases. *Acc. Chem. Res.* 2007; 40:466–474. [PubMed: 17518435]
- (10). Lee S-K, Nesheim JC, Lipscomb JD. Transient Intermediates of the Methane Monooxygenase Catalytic Cycle. *J. Biol. Chem.* 1993; 268:21569–21577. [PubMed: 8408008]



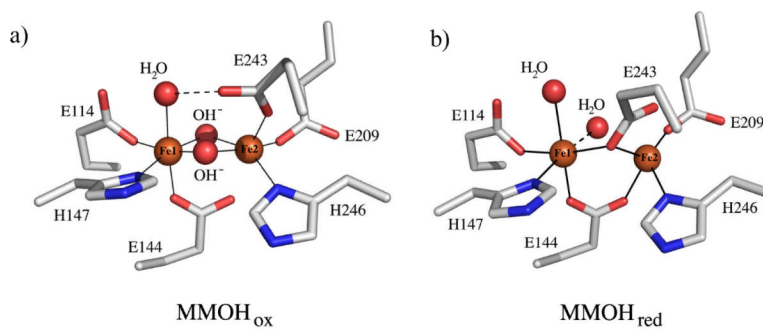
- (11). Liu KE, Valentine AM, Wang D, Huynh BH, Edmondson DE, Salifoglou A, Lippard SJ. Kinetic and Spectroscopic Characterization of Intermediates and Component Interactions in Reactions of Methane Monooxygenase from *Methylococcus capsulatus* (Bath). *J. Am. Chem. Soc.* 1995; 117:10174–10185.
- (12). Stahl SS, Francisco WA, Merckx M, Klinman JP, Lippard SJ. Oxygen Kinetic Isotope Effects in Soluble Methane Monooxygenase. *J. Biol. Chem.* 2001; 276:4549–4553. [PubMed: 11073959]
- (13). Bollinger JM Jr. Krebs C. Stalking Intermediates in Oxygen Activation by Iron Enzymes: Motivation and Method. *J. Inorg. Biochem.* 2006; 100:586–605. [PubMed: 16513177]
- (14). Gherman BF, Baik M-H, Lippard SJ, Friesner RA. Dioxygen Activation in Methane Monooxygenase: A Theoretical Study. *J. Am. Chem. Soc.* 2004; 126:2978–2990. [PubMed: 14995216]
- (15). Rinaldo D, Philipp DM, Lippard SJ, Friesner RA. Intermediates in Dioxygen Activation by Methane Monooxygenase: A QM/MM Study. *J. Am. Chem. Soc.* 2007; 129:3135–3147. [PubMed: 17326634]
- (16). *Myo*-inositol oxygenase, which activates O<sub>2</sub> at a mixed-valent diiron(II/III) center, utilizes a superoxodiiron(III) unit to oxidize *myo*-inositol. Xing G, Diao Y, Hoffart LM, Barr EW, Prabhu KS, Arner RJ, Reddy CC, Krebs C, Bollinger JM Jr. Evidence for C–H Cleavage by an Iron-Superoxide Complex in the Glycol Cleavage Reaction Catalyzed by *myo*-Inositol Oxygenase. *Proc. Natl. Acad. Sci. USA.* 2006; 103:6130–6135. [PubMed: 16606846]
- (17). Synthetic mixed-valent diiron(II/III) complexes can oxidize external substrates. Shan X, Que L Jr. Intermediates in the Oxygenation of a Nonheme Diiron(II) Complex, Including the First Evidence for a Bound Superoxo Species. *Proc. Natl. Acad. Sci. USA.* 2005; 102:5340–5345. [PubMed: 15802473] ; Zhao M, Helms B, Slonkina E, Friedle S, Lee D, DuBois J, Hedman B, Hodgson KO, Fréchet MJ, Lippard SJ. Iron Complexes of Dendrimer-Appended Carboxylates for Activating Dioxygen and Oxidizing Hydrocarbons. *J. Am. Chem. Soc.* 2008; 130:4352–4363. [PubMed: 18331028]
- (18). Liu KE, Wang D, Huynh BH, Edmondson DE, Salifoglou A, Lippard SJ. Spectroscopic Detection of Intermediates in the Reaction of Dioxygen with Reduced Methane Monooxygenase Hydroxylase from *Methylococcus capsulatus* (Bath). *J. Am. Chem. Soc.* 1994; 116:7465–7466.
- (19). H<sub>peroxo</sub> is denoted L in early studies of *Mc* MMOH and P in studies of *Mt* MMOH.
- (20). Shu L, Nesheim JC, Kauffmann K, Münck E, Lipscomb JD, Que L Jr. An Fe<sub>2</sub><sup>IV</sup>O<sub>2</sub> Diamond Core Structure for the Key Intermediate Q of Methane Monooxygenase. *Science.* 1997; 275:515–518. [PubMed: 8999792]
- (21). Valentine AM, Stahl SS, Lippard SJ. Mechanistic Studies of the Reaction of Reduced Methane Monooxygenase Hydroxylase with Dioxygen and Substrates. *J. Am. Chem. Soc.* 1999; 121:3876–3887.
- (22). We recently remeasured this value to be 0.75 s<sup>-1</sup>.
- (23). Brazeau BJ, Lipscomb JD. Kinetics and Activation Thermodynamics of Methane Monooxygenase Compound Q Formation and Reaction with Substrates. *Biochemistry.* 2000; 39:13503–13515. [PubMed: 11063587]
- (24). Tinberg CE, Lippard SJ. Revisiting the Mechanism of Dioxygen Activation in Soluble Methane Monooxygenase from *M. capsulatus* (Bath): Evidence for a Multi-Step, Proton-Dependent Reaction Pathway. *Biochemistry.* 2009; 48:12145–12158. [PubMed: 19921958]
- (25). Moënné-Loccoz P, Baldwin J, Ley BA, Loehr TM, Bollinger JM Jr. O<sub>2</sub> Activation by Non-Heme Diiron Proteins: Identification of a Symmetric  $\mu$ -1,2-Peroxide in a Mutant of Ribonucleotide Reductase. *Biochemistry.* 1998; 37:14659–14663. [PubMed: 9778340]
- (26). Skulan AJ, Brunold TC, Baldwin J, Saleh L, Bollinger JM Jr. Solomon EI. Nature of the Peroxo Intermediate of the W48F/D84E Ribonucleotide Reductase Variant: Implications for O<sub>2</sub> Activation by Binuclear Non-Heme Iron Enzymes. *J. Am. Chem. Soc.* 2004; 126:8842–8855. [PubMed: 15250738]
- (27). Moënné-Loccoz P, Krebs C, Herlihy K, Edmondson DE, Theil EC, Huynh BH, Loehr TM. The Ferroxidase Reaction of Ferritin Reveals a Diferric  $\mu$ -1,2 Bridging Peroxide Intermediate in Common with Other O<sub>2</sub>-Activating Non-Heme Diiron Proteins. *Biochemistry.* 1999; 38:5290–5295. [PubMed: 10220314]

- (28). Broadwater JA, Ai J, Loehr TM, Sanders-Loehr J, Fox BG. Peroxodiferric Intermediate of Stearoyl-Acyl Carrier Protein  $\Delta^9$  Desaturase: Oxidase Reactivity during Single Turnover and Implications for the Mechanism of Desaturation. *Biochemistry*. 1998; 37:14664–14671. [PubMed: 9778341]
- (29). Vu VV, Emerson JP, Martinho M, Kim YS, Münck E, Park MH, Que L Jr. Human Deoxyhypusine Hydroxylase, an Enzyme Involved in Regulating Cell Growth, Activates O<sub>2</sub> with a Nonheme Diiron Center. *Proc. Natl. Acad. Sci. USA*. 2009; 106:14814–14819. [PubMed: 19706422]
- (30). Bailey LJ, Fox BG. Crystallographic and Catalytic Studies of the Peroxide-Shunt Reaction in a Diiron Hydroxylase. *Biochemistry*. 2009; 48:8932–8939. [PubMed: 19705873]
- (31). These conclusions were based on modeling the active site  $2F_o - F_c$  difference density as H<sub>2</sub>O<sub>2</sub> by employing an O–O bond distance restraint of 1.5 Å; using this approach, the Fe–O bond distances are too long to assign the unit as a peroxodiiron(III) species. Attempts to release the restraint and refine the structure resulted in an increased O–O bond distance of 1.8 Å and decreased Fe–O bond distances of ~2.1 Å, neither of which support the peroxide formulation.
- (32). Tshuva EY, Lippard SJ. Synthetic Models for Non-Heme Carboxylate-Bridged Diiron Metalloproteins: Strategies and Tactics. *Chem. Rev*. 2004; 104:987–1012. [PubMed: 14871147]
- (33). Kim K, Lippard SJ. Structure and Mössbauer Spectrum of a ( $\mu$ -1,2-Peroxo)bis( $\mu$ -carboxylato)diiron(III) Model for the Peroxo Intermediate in the Methane Monooxygenase Hydroxylase Reaction Cycle. *J. Am. Chem. Soc*. 1996; 118:4914–4915.
- (34). Han W-G, Noodleman L. Structural Model Studies for the Peroxo Intermediate P and the Reaction Pathway from P  $\square$  Q of Methane Monooxygenase Using Broken-Symmetry Density Functional Calculations. *Inorg. Chem*. 2008; 47:2975–2986. [PubMed: 18366153]
- (35). Siegbahn PEM. O $\downarrow$ O Bond Cleavage and Alkane Hydroxylation in Methane Monooxygenase. *J. Biol. Inorg. Chem*. 2001; 6:27–45. [PubMed: 11191221]
- (36). Bochevarov AD, Li J, Song WJ, Friesner RA, Lippard SJ. Insights Into the Different Dioxygen Activation Pathways of Methane and Toluene Monooxygenase Hydroxylases. 2010 Manuscript in Preparation.
- (37). Beauvais LG, Lippard SJ. Reactions of the Peroxo Intermediate of Soluble Methane Monooxygenase Hydroxylase with Ethers. *J. Am. Chem. Soc*. 2005; 127:7370–7378. [PubMed: 15898785]
- (38). Tinberg CE, Lippard SJ. Oxidation Reactions Performed by Soluble Methane Monooxygenase Hydroxylase Intermediates H<sub>peroxo</sub> and Q Proceed by Distinct Mechanisms. *Biochemistry*. 2010; 49:7902–7912. [PubMed: 20681546]
- (39). Lee S-K, Fox BG, Froland WA, Lipscomb JD, Münck E. A Transient Intermediate of the Methane Monooxygenase Catalytic Cycle Containing an Fe<sup>IV</sup>Fe<sup>IV</sup> Cluster. *J. Am. Chem. Soc*. 1993; 115:6450–6451.
- (40). Xue G, Wang D, De Hont R, Fiedler AT, Shan X, Münck E, Que L Jr. A Synthetic Precedent for the [Fe<sup>IV</sup><sub>2</sub>( $\mu$ -O)<sub>2</sub>] Diamond Core Proposed for Methane Monooxygenase Intermediate Q. *Proc. Natl. Acad. Sci. USA*. 2007; 104:20713–20718. [PubMed: 18093922]
- (41). Rowe GT, Rybak-Akimova EV, Caradonna JP. Unraveling the Reactive Species of a Functional Non-Heme Iron Monooxygenase Model Using Stopped-Flow UV-Vis Spectroscopy. *Inorg. Chem*. 2007; 46:10594–10606. [PubMed: 17988120]
- (42). Xue G, De Hont R, Münck E, Que L Jr. Million-Fold Activation of the [Fe<sub>2</sub>( $\mu$ -O)<sub>2</sub>] Diamond Core for C–H Bond Cleavage. *Nat. Chem*. 2010; 2:400–405. [PubMed: 20414242]
- (43). Ambundo EA, Friesner RA, Lippard SJ. Reactions of Methane Monooxygenase Intermediate Q with Derivatized Methanes. *J. Am. Chem. Soc*. 2002; 124:8770–8771. [PubMed: 12137510]
- (44). Baik M-H, Newcomb M, Friesner RA, Lippard SJ. Mechanistic Studies on the Hydroxylation of Methane by Methane Monooxygenase. *Chem. Rev*. 2003; 103:2385–2419. [PubMed: 12797835]
- (45). Denisov IG, Makris TM, Sligar SG, Schlichting I. Structure and Chemistry of Cytochrome P450. *Chem. Rev*. 2005; 105:2253–2277. [PubMed: 15941214]
- (46). The pD values of the buffers employed in these experiments were uncorrected for deuterium isotope effect.

- (47). Lee S-K, Lipscomb JD. Oxygen Activation Catalyzed by Methane Monooxygenase Hydroxylase Component: Proton Delivery during the O-O Bond Cleavage Steps. *Biochemistry*. 1999; 38:4423–4432. [PubMed: 10194363]
- (48). Do LH, Hayashi T, Moëne-Loccoz P, Lippard SJ. Carboxylate as the Protonation Site in (Peroxo)diiron(III) Model Complexes of Soluble Methane Monooxygenase and Related Diiron Proteins. *J. Am. Chem. Soc.* 2010; 132:1273–1275. [PubMed: 20055391]
- (49). Jensen KP, Bell CB III, Clay MD, Solomon EI. Peroxo-Type Intermediates in Class I Ribonucleotide Reductase and Related Binuclear Non-Heme Iron Enzymes. *J. Am. Chem. Soc.* 2009; 131:12155–12171. [PubMed: 19663382]
- (50). Bollinger JM Jr, Krebs C, Vicol A, Chen S, Ley BA, Edmondson DE, Huynh BH. Engineering the Diiron Site of *Escherichia coli* Ribonucleotide Reductase Protein R2 to Accumulate an Intermediate Similar to  $H_{\text{peroxo}}$ , the Putative Peroxodiiron(III) Complex from the Methane Monooxygenase Catalytic Cycle. *J. Am. Chem. Soc.* 1998; 120:1094–1095.
- (51). Broadwater JA, Achim C, Münck E, Fox BG. Mössbauer Studies of the Formation and Reactivity of a Quasi-Stable Peroxo Intermediate of Stearoyl-Acyl Carrier Protein  $\Delta^9$ -Desaturase. *Biochemistry*. 1999; 38:12197–12204. [PubMed: 10493786]
- (52). Pereira AS, Small W, Krebs C, Tavares P, Edmondson DE, Theil EC, Huynh BH. Direct Spectroscopic and Kinetic Evidence for the Involvement of a Peroxidiferic Intermediate during the Ferroxidase Reaction in Fast Ferritin Mineralization. *Biochemistry*. 1998; 37:9871–9876. [PubMed: 9665690]
- (53). Zhang X, Furutachi H, Fujinami S, Nagatomo S, Maeda Y, Watanabe Y, Kitagawa T, Suzuki M. Structural and Spectroscopic Characterization of ( $\mu$ -Hydroxo or  $\mu$ -Oxo)( $\mu$ -peroxo)diiron(III) Complexes: Models for Peroxo Intermediates of Non-Heme Diiron Proteins. *J. Am. Chem. Soc.* 2005; 127:826–827. [PubMed: 15656607]
- (54). Dong Y, Zang Y, Shu L, Wilkinson EC, Que L Jr, Kauffmann K, Münck E. Models for Nonheme Diiron Enzymes. Assembly of a High-Valent  $Fe_2(\mu-O)_2$  Diamond Core from Its Peroxo Precursor. *J. Am. Chem. Soc.* 1997; 119:12683–12684.
- (55). Dong Y, Fujii H, Hendrich MP, Leising RA, Pan G, Randall CR, Wilkinson EC, Zang Y, Que L Jr, Fox BG, Kauffmann K, Münck E. A High-Valent Nonheme Iron Intermediate. Structure and Properties of  $[Fe_2(\mu-O)_2(5-Me-TPA)_2](ClO_4)_3$ . *J. Am. Chem. Soc.* 1995; 117:2778–2792.
- (56). Dong Y, Que L Jr, Kauffmann K, Münck E. An Exchange-Coupled Complex with Localized High-Spin  $Fe^{IV}$  and  $Fe^{III}$  Sites of Relevance to Cluster X of *Escherichia coli* Ribonucleotide Reductase. *J. Am. Chem. Soc.* 1995; 117:11377–11378.
- (57). Hsu H-F, Dong Y, Shu L, Young V Jr, Que L Jr. Crystal Structure of a Synthetic High-Valent Complex with an  $Fe_2(\mu-O)_2$  Diamond Core. Implications for the Core Structures of Methane Monooxygenase Intermediate Q and Ribonucleotide Reductase Intermediate X. *J. Am. Chem. Soc.* 1999; 121:5230–5237.

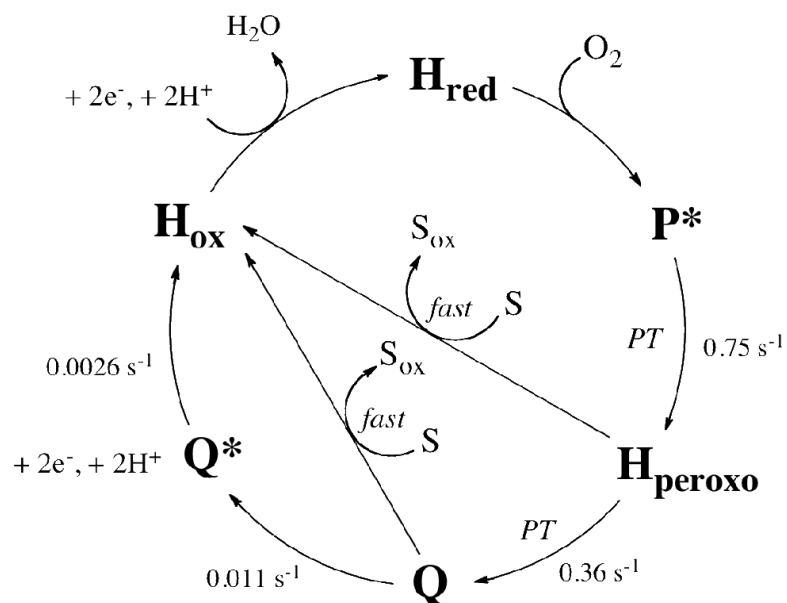
**Scheme 1.**

Proposed Models Describing the Role of Protons During MMOH O<sub>2</sub> Activation.

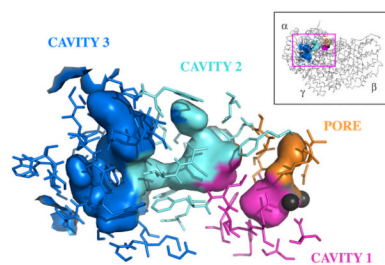


**Figure 1.** Diiron active site structures of (a) *Mc* MMOH<sub>ox</sub> (PDB ID 1MTY) and (b) *Mc* MMOH<sub>red</sub> (PDB ID 1FYZ).

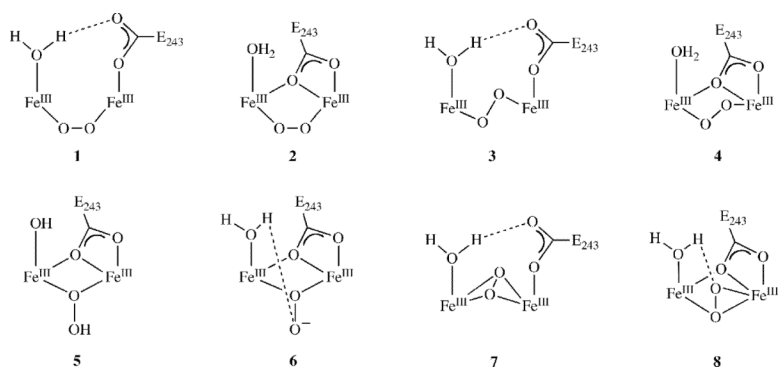




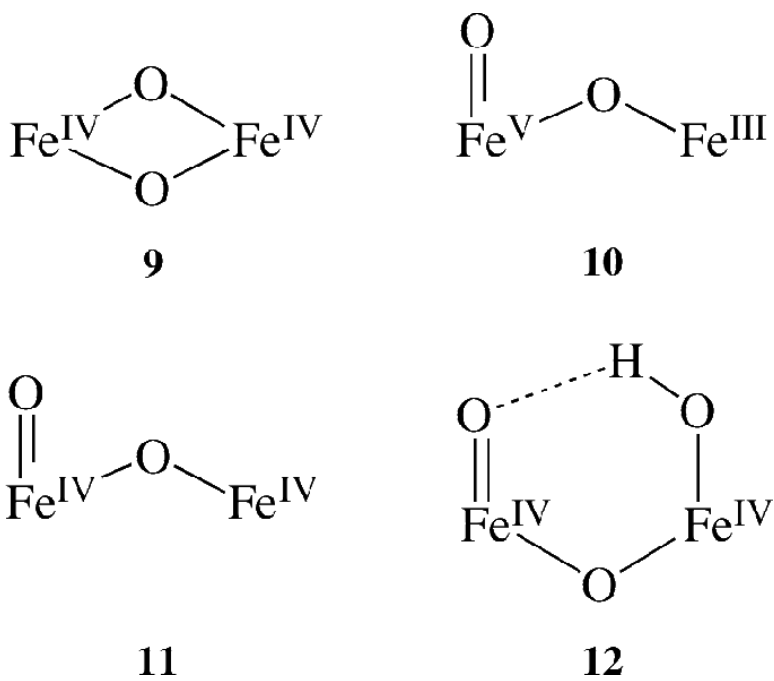
**Figure 2.** *Mc* MMOH catalytic cycle. Rate constants were measured at pH 7.0 and 4 °C. S denotes substrate.



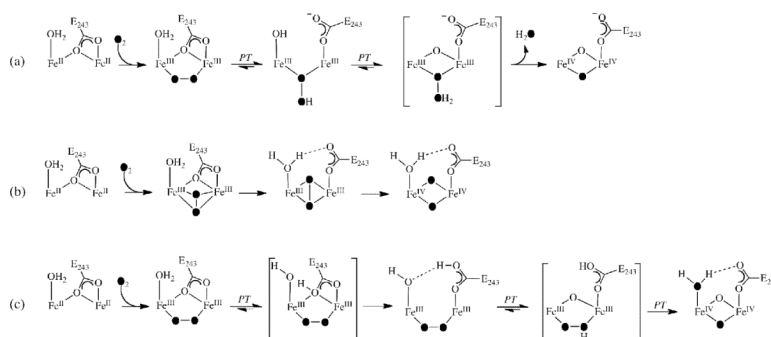
**Figure 3.** Pathways of substrate ingress in MMOH. Three hydrophobic cavities link the diiron center to the protein exterior. A small pore lined by hydrophilic residues also leads to the protein surface. PDB 1MTY.



**Figure 4.**  
Possible Structures for the Peroxodiiron(III) Species of MMOH.



**Figure 5.**  
Possible structures for  $\{\text{Fe}_2\text{O}_2\}^{4+}$  core of Q.

**Figure 6.**

Three proposed mechanisms for Q formation. (a) Proton-assisted heterolytic O–O bond cleavage involving a stable hydroperoxide intermediate. (b) Proton-independent homolytic O–O bond cleavage. (c) Proton-assisted heterolytic O–O bond cleavage involving protonation and rearrangement of E<sub>243</sub> prior to Q formation.



**Table 1**  
Spectroscopic Parameters of Peroxodiiron(III) Intermediates of Enzymes and Model Complexes

	optical		Mössbauer		Peroxide Binding Mode
	$\lambda_{\max}$ (nm)	$\epsilon$ ( $M^{-1} \text{ cm}^{-1}$ )	$\delta$ (mm/s)	$\Delta E_Q$ (mm/s)	
MMOH $H_{\text{peroxo}}$ ( <i>Mc</i> )	420; 720	3880; 1350 <sup>a</sup>	0.66	1.51 <sup>b</sup>	-
MMOH $H_{\text{peroxo}}$ ( <i>Mt</i> )	725	2500 <sup>c</sup>	0.67	1.51 <sup>d</sup>	-
RNR-R2 D84E	700	1500 <sup>e</sup>	0.63	1.58 <sup>e</sup>	$\mu$ -1,2 <sup>f</sup>
$\Delta^9$ -desaturase	700	1200 <sup>g</sup>	0.68; 0.64	1.90; 1.06 <sup>g</sup>	$\mu$ 1,2 <sup>h</sup>
frog M ferritin	650 <sup>i</sup>	-	0.62	1.08 <sup>i</sup>	$\mu$ 1,2 <sup>j</sup>
hDOHH <sup>k</sup>	630	2800	0.55; 0.58	1.16; 0.88	$\mu$ -1,2
$[\text{Fe}_2(\mu$ -1,2- $\text{O}_2)(\mu$ - $\text{O}_2\text{CCH}_2\text{Ph})_2(\text{HB}(\text{pz})_3)_2]$ <sup>l</sup>	694	2650	0.66	1.40	gauche $\mu$ -1,2
$[\text{Fe}_2(\mu$ -OH)( $\mu$ -1,2- $\text{O}_2$ )(6- $\text{Me}_2$ -BPP) <sub>2</sub> ] <sup>+</sup> <sup>m</sup>	644	3000	0.50	1.31	<i>cis</i> - $\mu$ -1,2
$[\text{Fe}_2(\mu$ -O)( $\mu$ -1,2- $\text{O}_2$ )(6- $\text{Me}_3$ -TPA) <sub>2</sub> ] <sup>2+</sup> <sup>n</sup>	494; 648	1100; 1200	0.54	1.68	<i>cis</i> - $\mu$ -1,2

These studies were performed on the D84E/W48F variant.

*pz*' = 3,5-bis(isopropyl)pyrazolyl.

BPP = N,N-bis(2-pyridylmethyl)-3-aminopropionate.

TPA = ris(2-pyridylmethyl)amine.

<sup>a</sup>Ref 24.

<sup>b</sup>Ref 11.

<sup>c</sup>Ref 47.

<sup>d</sup>Ref 20.

<sup>e</sup>Ref 50.

<sup>f</sup>Ref 25.

<sup>g</sup>Ref 51.

<sup>h</sup>Ref 28.

<sup>i</sup>Ref 52.

<sup>j</sup>Ref 27.

<sup>k</sup>Ref 29.

<sup>l</sup>Ref 33.

<sup>m</sup>Ref 53.

<sup>n</sup>Ref 54.

NIH-PA Author Manuscript

NIH-PA Author Manuscript

NIH-PA Author Manuscript

**Table 2**  
Spectroscopic Parameters of Intermediate Q and High-Valent Model Complexes

	optical		Mössbauer		
	$\lambda_{\max}$ (nm)	$\epsilon$ ( $M^{-1} \text{ cm}^{-1}$ )	$\delta$ (mm/s)	$\Delta E_Q$ (mm/s)	Fe-Fe(Å)
MMOH Q (Mc)	420	8415 <sup>a</sup>	0.21; 0.14	0.68; 0.55 <sup>b</sup>	-
MMOH Q (Mt)	330; 430	7500; 7500 <sup>c</sup>	0.17	0.53 <sup>d</sup>	2.46 <sup>e</sup>
[Fe <sub>2</sub> ( $\mu$ -O) <sub>2</sub> (L) <sub>2</sub> ] <sup>2+</sup>	366; 616	7900; 5200 <sup>f</sup>	0.48; 0.08	1.6; 0.5 <sup>g</sup>	2.683 <sup>h</sup>
[Fe <sub>2</sub> ( $\mu$ -O) <sub>2</sub> (L) <sub>2</sub> ] <sup>1+</sup> <sup>i</sup>	485; 875	9800; 2200	-0.04	2.09	2.73

L = 5-Me<sub>3</sub>-TPA; TPA = tris(2-pyridylmethyl)amine.

L = 6-Me<sub>3</sub>-TPA.

L = 5-Et<sub>3</sub>-TPA.

L = tris((4-methoxy-3,5-dimethylpyrid-2-yl)d<sub>2</sub>-methyl)amine.

<sup>a</sup>Ref 24.

<sup>b</sup>Ref 11.

<sup>c</sup>Ref 10.

<sup>d</sup>Ref 39.

<sup>e</sup>Ref 20.

<sup>f</sup>Ref 55.

<sup>g</sup>Ref 56.

<sup>h</sup>Ref 57.

<sup>i</sup>Ref 40.